Mechanism of the photocatalytic activity of p-Si(100)/n-ZnO nanorods heterojunction

Nguyen Thi Hoa, Vuong Van Cuong, Nguyen Dinh Lam[*]

Department of Physics, Hanoi National University of Education, 136, Xuanthuy, Caugiay, Hanoi, Vietnam

HIGHLIGHTS

- A heterojunction of p-Si/n-ZnO NRs was fabricated by a simple hydrothermal method.
- An improvement in photocatalytic activity of the heterojunction was demonstrated.
- The enhancement is attributed to the inner electric field and effective surface area.
- This heterojunction serves as a convenient recyclable and effective photocatalyst.

ARTICLE INFO

ABSTRACT

A heterojunction of p-Si(100)/n-ZnO nanorods was fabricated by a simple hydrothermal method. The photocatalytic activity of this heterojunction was examined by degradation of Rhodamine B (RhB) under UV light irradiation. The results indicated that the p-Si(100)/n-ZnO nanorods heterojunction exhibits higher photocatalytic activity compared to that of a glass/n-ZnO nanorods. The inner electric field created by the space charge region of heterojunction will oppose the recombination of photogenerated electrons and holes. Furthermore, this heterojunction serves as a convenient recyclable and effective photocatalyst. The photodecomposition rate of RhB after 5 cycles is negligible change in an experiment using this heterojunction.

1. Introduction

Zinc oxide (ZnO) nanostructures have been considered as a promising candidate for application in photocatalysis because of their specific surface area, high electron mobility, and high photosensitivity [1–5]. Furthermore, ZnO nanostructures are usually fabricated on some kinds of substrates, thus, they are easily separated from a solution and recycled for waste water treatment. However, the efficiency of pure ZnO photocatalyst is still low because of the rapid recombination of the photogenerated electrons and holes that is attributed to the direct bandgap characteristic of ZnO semiconductor. To solve this issue, noble metals such as Ag [6,7], Au [8], and Pt [9], or some metal oxides [10–12] were decorated onto ZnO nanostructure where noble metals and metal oxides are utilized to collect photogenerated electrons and reduce the recombination of the photogenerated carriers. Moreover, using an ITO layer as a photogenerated electron collecting layer is also another way to separate photogenerated electron-hole pairs [13]. Due to band alignment of ITO and ZnO, the ITO/ZnO junction can separate the photo-generated electrons and holes and the recombination of electron-hole pairs is suppressed. The results indicated that the ZnO nanowire with an ITO layer exhibits notably enhanced photocatalytic activity, which was 9.65 times faster than that of ZnO nanowire without an ITO layer. In addition, the organic molecules are mainly oxidized by holes concentrated in the valence band of ZnO because the surface of the ITO layer is covered by an Al doped ZnO seed layer.

Moreover, ZnO can only be activated by ultraviolet light due to its wide band gap (3.37eV). That means it can absorb less than 5% of sunlight and thus restricts the practical application of ZnO photocatalysts. Therefore, significant progresses have been made to effectively utilize the visible light ($\lambda > 420$ nm). One of the widely used strategies to extend the photoresponse of a wide bandgap semiconductor towards the visible spectral region is combining wide bandgap semiconductors with narrow bandgap semiconductors such as CuS [14], Cu_2O [15]. Both materials were proven

to be efficient visible light driven photocatalysts. Silicon (Si) is a narrow indirect bandgap semiconductor (1.12 eV). p-Si/n-ZnO film and p-Si/n-ZnO nanorods (ZnO NRs) heterojunctions were already fabricated by various methods and mainly applied to photovoltaic [16–19]. In photocatalytic applications, an ultralong ZnO nanowire array grown on Si substrate by vapor transport was reported [20]. The result showed an enhancement in photocatalytic activity of ZnO nanowires on the Si substrate compared to that of ZnO nanowires on the glass substrate. However, in this work, the role of the p-Si/ZnO heterojunction hasn't been mentioned. Based on this heterojunction, photogenerated charge carriers can be separated by an inner electric field and the optical absorption range of this photocatalyst can be extended. Therefore, further investigations of the p-Si/ZnO NRs heterojunction in photocatalytic activity are still required.

In this work, p-Si/n-ZnO film and p-Si/n-ZnO NRs heterojunctions were fabricated by spin coating and simple hydrothermal methods, respectively. As comparison, ZnO film and ZnO NRs were also fabricated on glass substrates by the same process. The photocatalytic activities of these samples have been investigated. The results demonstrated that the p-Si/n-ZnO NRs heterostructure exhibited enhanced photocatalytic activities compared to the glass/n-ZnO NRs. The enhanced photocatalytic mechanism of p-Si/n-ZnO NRs heterostructure would be ascribed to the extension of the optical absorption range and the efficient separation of photogenerated electron-hole pairs.

2. Experimental details

2.1. Materials

$Zn(NO_3)_2.6H_2O$, hexamethylenetetramine ($C_6H_{12}N_4$) are all purchased from Sigma. All chemicals are of analytic reagent grade and used as received without purification. Glass and p-Si wafers were used as the substrates to support the ZnO nanorods. Before the ZnO NRs growth, the substrates (2 cm × 2 cm × 0.1 cm) were cleaned by 5% NaOH solution, methanol, and deionized water in sequence.

2.2. Synthesis of ZnO film and ZnO NRs

ZnO NRs were fabricated on glass and p-Si substrates coated with a seed layer of ZnO nanoparticles by a simple hydrothermal method. The ZnO nanoparticles seed layer was deposited by uniformly spin coating. In the process of hydrothermal growth of ZnO NRs, a growth solution was prepared using 20 mM zinc nitrate hexahydrate and 20 mM hexamethylenetetramine. 100 mL solution was then transferred into Teflon-lined stainless steel autoclave. Afterward, the glass or p-Si substrates coated with a seed layer were immersed into the growth solution and heated to 80 °C for 120 min. Finally, the autoclaves were allowed to cool down naturally. The obtained samples were cleaned ultrasonically in ethanol and distilled water for 30 min, followed by a drying treatment at 100 °C. Schematic illustration of the p-Si/ZnO NRs heterojunction is shown in Fig. 1(a).

For comparison purpose, 300 nm thick of ZnO films were also fabricated on glass and p-Si substrates by spin coating technique. 0.3 M zinc acetate dehydrate ($Zn(CH_3COO).2H_2O$) as a precursor, isopropanol (IPA) as a solvent and diethanolamine (DEA) as a stabilizer were utilized to create a solution. The obtained solution was spread on the substrates using a spin coating system at a spin speed of 3000 rpm and spin time of 30 s. The films were then dried at 150 °C for 20 min in an oven to evaporate the solvent and remove organic residuals. The spin-coating and drying processes were repeated five times to get a desired thickness and then the
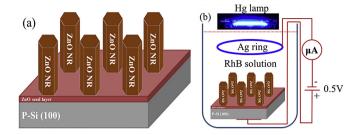

Fig. 1. Schematic illustration of (a) a p-Si/ZnO NRs heterojunction and (b) photocurrent response measurement.

precursor films were annealed at 500 °C for 1 h in air.

2.3. Characterization

The surface morphologies were characterized using a field emission scanning electron microscopy (FESEM, Hitachi, S-4800). The crystal phases of the fabricated samples were determined using an X-ray diffractometer (XRD) D5000 with CuKα radiation ($\lambda = 1.5406$ Å) over the 2θ range 20–70° at room temperature. The UV−Vis transmittance and absorption spectra were measured by a UV-Vis spectrophotometer (Jasco, V-670).

2.4. Photocatalytic activity measurement

The photocatalytic activity of the fabricated samples was investigated by a degradation of Rhodamine B (RhB) under ultraviolet (UV) light irradiation. A sample (the area is 2 cm × 2 cm) was placed in 100 ml RhB solution whose initial concentration was 5 mg L^{-1}. The reactor was kept in the dark for 30 min to allow adsorption-desorption equilibrium before light irradiation. A 250 W mercury lamp with a UV bandpass filter was served as a UV light source and placed about 30 cm from the reactor to minimize the heat effect. After given time intervals (10 min), 3 mL of solution was withdrawn and analyzed by a UV-Vis spectrophotometer (Jasco, V-670) at a wavelength of 554 nm. For the reusability test of the p-Si/n-ZnO NR heterojunction, optical absorptions of RhB solution at the wavelength of 554 nm were taken before and after irradiation for 60 min. After each cycle, the p-Si/ZnO NRs was rinsed to remove residual molecules and immersed into a fresh solution of the same concentration and volume. This process was repeated for 5 times to confirm the suitability for multiple uses of the p-Si/n-ZnO NRs photocatalyst. Furthermore, the photocatalytic activity of this heterojunction under natural sunlight was also tested. In this test, three cups containing of 100 ml of 5 mg.L^{-1} RhB solution with and without placing the p-Si/n-ZnO NRs heterojunction, the glass/n-ZnO NRs were irradiated by nature sunlight for 10 h at the same position. The concentrations of RhB solution were analyzed based on the change of the absorption peak intensity at 554 nm.

In order to understand the role of the heterojunction in the photocatalytic activity, the photocurrent response was carried out. The photocurrent response is measured using a homemade setup with a Keithley 2000 multimeter, a DC supply source, and a 250 W mercury lamp. This measurement setup was depicted in Fig. 1(b).

3. Results and discussion

3.1. Structural characteristics

Fig. 2 shows SEM images of the ZnO film and ZnO NRs grown on glass substrates. Fig. 2(a) indicated that ZnO film is made up of tens-nanometer particles and the thickness of the film is about 300 nm
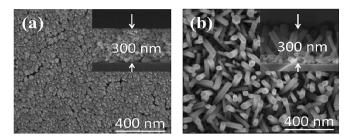
Fig. 2. Top- and side-view SEM images of (a) ZnO film and (b) ZnO NRs grown on glass substrates.

as shown in cross-section image (inset in Fig. 2(a)). Well-aligned and uniformly distributed ZnO NRs is observed in Fig. 2(b). The SEM image of this sample indicates that an average length, diameter, and density of ZnO NRs are approximately of 300 nm, 40 nm, and 1.5×10^{10} rods/cm^2, respectively.

Fig. 3(a) shows the XRD patterns of the ZnO film and ZnO NRs grown on glass substrates. The XRD patterns indicate that the structure of the fabricated samples is polycrystalline. The presence of the (100), (002), (101), (102), (110), (103), and (112) peaks in the XRD patterns also indicates hexagonal wurtzite structure of ZnO. Diffraction peaks related to other impurity phases are not observed in the XRD patterns. The much higher intensity of the (002) diffraction peaks for ZnO NRs indicates the excellent c-axis orientation of this sample. Fig. 3(b) shows the optical transmittance spectra of the ZnO film and ZnO NRs grown on glass substrates measured in the wavelength range 300–800 nm at room temperature. The average optical transmittance of the samples in the visible region is higher than 80%. For estimating the band gap energy (E_g) of the samples, $(\alpha h\nu) = \beta(h\nu - E_g)^m$ relationship is utilized [15]. Where, α is the absorption coefficient, β is a constant and $h\nu$ is the photo energy. The ZnO is a direct band gap semiconductor so m is chosen as ½ [21]. The absorption coefficient α of the films is calculated from the transmittance spectra using the equation of $\alpha = \frac{1}{t}\ln\left(\frac{1}{T}\right)$, where t is the thickness of film and T is the transmittance. The band gap energy E_g of about 3.27 eV for the ZnO film and ZnO NRs is determined by extrapolating the linear region of $(\alpha h\nu)^2$ versus the photo energy (inset in the Fig. 3 (b)).

3.2. Photocatalytic properties

The photocatalytic activity of the p-Si/n-ZnO NRs heterostructure was evaluated by the bleaching of RhB dye under the irradiation of an Hg lamp. During the photodegradation process, the concentration change was characterized by the RhB absorption peak at 554 nm using a UV − vis spectrometer as shown in Fig. 4(a).
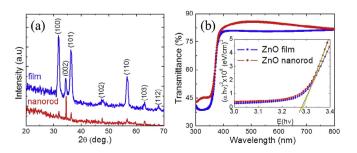

Fig. 3. (a) XRD patterns of the ZnO film and ZnO NRs grown on glass substrates. (b) Optical transmittance spectra of the ZnO film and ZnO NRs grown on glass substrates. The inset shows a plot of $(\alpha h\nu)^2$ versus $h\nu$ for estimation of optical band gap of the ZnO film and ZnO NRs grown on glass substrates.

C and Co in Fig. 4 are reaction concentration and initial concentration after the equilibrium adsorption of the RhB, respectively. From −30 to 0 min, the aqueous solution of RhB was kept in dark for ensuring an adsorption/desorption equilibrium of RhB on the fabricated samples. Adsorption and self-degradation aren't observed at this time. The concentration of RhB is reduced when reaction time increases under the illumination of UV light. After 60 min illumination, the degradation of RhB concentrations by the glass substrate, Si substrate, glass/ZnO film, glass/ZnO NR, p-Si/ZnO film, and p-Si/ZnO NR is 35, 40, 56, 68, 83, and 93%, respectively. This result indicated that the controlled experiment with the glass substrate shows a considerable degradation of RhB. This might be attributed to the self-degradation of RhB under UV irradiation. Moreover, the first-order kinetics of RhB photodegradation was depicted in Fig. 4(b). The pseudo-order rate constant (k) was determined from the slope of the line and shown in Fig. 4(b) (inset). The result indicated that the k value of p-Si/ZnO NRs in degrading RhB is 3 times higher compared to that of glass/ZnO NRs. This enhancement in photocatalytic activity of ZnO fabricated on p-Si substrates can be explained by the contribution of the inner electric field to the separation of photogenerated electron-hole pairs. Furthermore, the effective surface area of about 22 cm^2 can be determined for the p-Si/ZnO NRs sample. Therefore, the higher degradation rate of RhB molecules by p-Si/ZnO NR compared to that by p-Si/ZnO film can be attributed to the larger effective surface area of ZnO NRs.

Fig. 5 shows the degradation of RhB concentrations by the p-Si/ZnO NRs sample when it is irradiated on the ZnO NRs and the Si sides. The degradation of RhB concentration by the p-Si substrate is also depicted in Fig. 5 for comparison purpose. When the p-Si/ZnO NRs sample is illuminated on the p-Si side, the photocatalytic activity is lower than that illuminated on the ZnO NR side and higher than that of the p-Si substrate. The reduction in photocatalytic activity of this sample when it is illuminated on the p-Si side might be attributed to the thickness of the p-Si substrate (~300 μm). Photogenerated electron-hole pairs at the back side surface of the p-Si substrate might be easily recombined before they are separated by the inner electric field of the p-n heterojunction. In addition, the effective surface area of the ZnO NRs is larger than that of the p-Si. Therefore, the degradation rate of RhB concentration by the p-Si/ZnO NRs irradiated on the ZnO NRs side is faster than that irradiated on that p-Si side. Moreover, based on the degradation rate of RhB concentration by the p-Si substrate, the role of the p-n heterojunction in photocatalytic activity is demonstrated.

Fig. 6 shows the photocatalytic degradation cycles of RhB. For each cycle of the photodecomposition experiment, the p-Si/ZnO NRs are rinsed to remove residual molecules and immersed into a fresh solution of the same concentration and volume. After 5 cycles, a negligible change in the photodecomposition rate is observed. This result demonstrates that the p-Si/ZnO NR is high photostable and reusable photocatalyst.

The photocatalytic activity of this heterojunction under natural sunlight was also evaluated as illustrated in Fig. 7. After exposure to 10 h of bright sunlight, about 70% of RhB was decomposed by the p-Si/ZnO NRs heterojunction while only a small change in the UV − vis absorption spectrum of RhB using the glass/ZnO NRs. This result indicates the extension of optical absorption range and the excellent photocatalytic ability of this heterojunction with natural sunlight.

3.3. Mechanism of the enhanced photocatalytic activity of p-Si/ZnO NRs

The I−V characteristic of the p-Si/ZnO NRs exhibits diode-like-rectifying-behavior as shown in Fig. 8(a). This result indicates
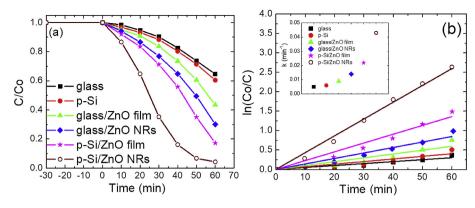
Fig. 4. (a) Photodegradation of RhB under UV light by different samples and (b) the first-order kinetic plot for RhB photodegredation.
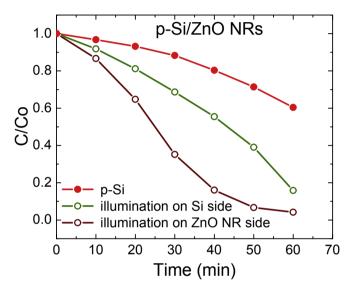

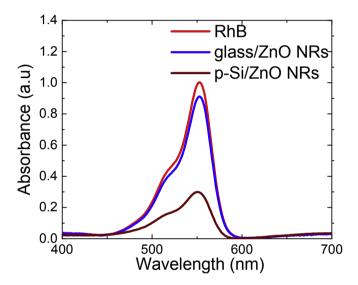**Fig. 5.** The photodegradation of RhB by the p-Si/ZnO NRs heterojunction when it is irradiated on ZnO NRs and Si sides.

Fig. 7. Optical absorption spectra of RhB after 10 h irradiated by natural sunlight with different samples.
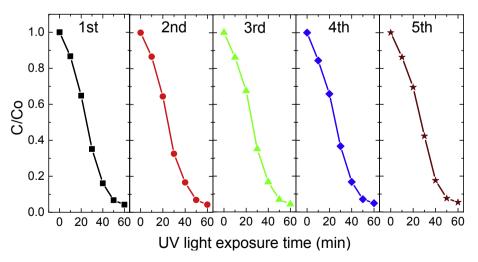

Fig. 6. The photocatalytic degradation cycles of RhB by p-Si/ZnO NRs over 5 cycles.

that the p-Si/ZnO NRs heterojunction can be well formed under our experimental condition. Furthermore, the normalized photocurrent response of the p-Si/ZnO NRs photocatalyst is also studied. The measurement setup is described in Fig. 1(b). The result is shown in

Fig. 8(b) with two cases of applied potential bias: positive to the p-Si [(+) p-Si] and negative to the p-Si [(−) p-Si]. The applied voltage is 0.5 V during the irradiation process. The rise and fall of the photocurrents correspond well to the UV illumination being
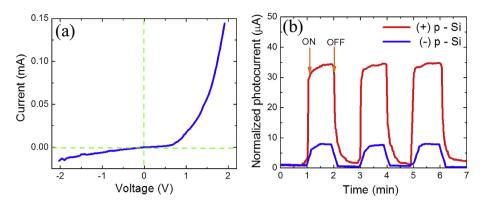
Fig. 8. (a) The I–V characteristic of the p-Si/ZnO NRs and (b) the normalized photocurrent response of the p-Si/ZnO NRs photocatalyst.

switched on and off for the both cases. This result indicates that the p-Si/ZnO NR photocatalyst shows a high photoresponse. Moreover, a higher photocurrent of (+) p-Si compared to that of (−) p-Si is attributed to the characteristic of the p-n heterojunction.

The enhancement photocatalytic activity of the p-Si/ZnO NRs photocatalyst can be explained by the heterojunction formation between the p-Si and the n-ZnO NRs. When the p-Si and the n-ZnO closely contact with each other, they should have same Fermi level, leading to the shift of their conduction and valence bands [22,23]. An inner electric field forms at the junction. An approximate equilibrium energy band diagram and schematic diagram for the p-Si/ZnO NRs heterojunction is shown in Fig. 9. When the p-Si/ZnO NRs heterojunction is irradiated with photon energies higher or equal to the band gaps of ZnO and Si, electron-hole pairs are generated (Eq. (1)). Under the action of the inner electric field, the photogenerated electrons can be injected from the p-Si conduction band to that of the ZnO NRs. In the valence band, the photogenerated holes migrate to the opposite direction. Subsequently,
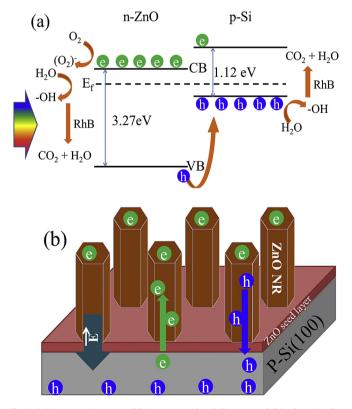
the photogenerated electrons can be easily trapped by the adsorbed O_2 molecules to produce superoxide radical anions of $(O_2)^-$ (Eq. (2)). The $(O_2)^-$ radicals and electrons can then react with H_2O to create -OH radicals (Eq. (3)). The photogenerated holes in valence band of Si can be scavenged by the H_2O molecules to producte -OH (Eq. (4)). These -OH are responsible for degradation of RhB molecules (Eq. (5)). These processes can be proposed as the following equations.

$$p\text{-Si/ZnO NR} + h\nu \rightarrow p\text{-Si/ZnO NR } (h^+ + e^-) \tag{1}$$

$$e^- + O2 \rightarrow (O_2)^- \tag{2}$$

$$(O_2)^- + 2H_2O + e^- \rightarrow \text{-OH} + 3OH^- \tag{3}$$

$$h^+ + OH^- \rightarrow \text{-OH} \tag{4}$$

$$\text{-OH} + RhB \rightarrow CO_2 + H_2O \tag{5}$$

Based on this technique, the photogenerated electrons and holes are efficiently separated and the recombination of electron-hole pairs is suppressed. Furthermore, the electrons and holes will take the same role in photodegradation process. However, further study including quantum efficiency analysis will be necessary to fully understand the photocatalysis mechanism of p-Si/ZnO NRs.

4. Conclusions

The p-Si/ZnO NR heterojunction has been successfully fabricated by a simple hydrothermal method. After 60 min illumination, the degradation of RhB concentrations by the p-Si/ZnO NR can be reached to 93% that is about 1.3 times higher compared to that of the glass/ZnO NR. Moreover, the pseudo-order rate constant (k) of p-Si/ZnO NRs in degrading RhB is 3 times higher compared to that of glass/ZnO NRs. This enhancement in photocatalytic activity was attributed to the inner electric field formed in the heterojunction. The heterojunction has also demonstrated to work as effective and recyclable photocatalyst and exhibit excellent photocatalytic activity under natural sunlight. Therefore, using a heterojunction between low and high bandgap energy semiconductor materials is an efficient method to improve the activity of semiconductor photocatalysts.

Fig. 9. (a) An approximate equilibrium energy band diagram and (b) schematic diagram for the p-Si/ZnO NRs heterojunction.

References

[1] J. Xie, H. Wang, M. Duan, L. Zhang, Appl. Surf. Sci. 257 (15) (2011) 6358—6363.
[2] C. Wu, L. Shen, H. Yu, Q. Huang, Y.C. Zhang, Mater. Res. Bull. 46 (7) (2011) 1107—1112.
[3] F. Xu, Y. Shen, L. Sun, H. Zeng, Y. Lu, Nanoscale 3 (2011) 5020—5025.
[4] T.V.A. Kusumam, T. Panakka, T. Divya, M.P. Nikhila, M. Anju, K. Anas, N.K. Renuka, Ceram. Int. 42 (3) (2016) 3769—3775.
[5] A. Mardiroosi, A.R. Mahjoub, H. Fakhri, J. Mater. Sci. Mater. Electron. 28 (2017) 11722—11732.
[6] M.J. Sampaio, M.J. Lima, D.L. Baptista, A.M.T. Silva, C.G. Silva, J.L. Faria, Chem. Eng. J. (2016). https://doi.org/10.1016/j.cej.2016.05.105.
[7] Y. Liang, N. Guo, L. Li, R. Li, G. Ji, S. Gan, New J. Chem. 40 (2016) 1587—1594.
[8] M.J. Sampaio, J.W.L. Oliveira, C.I.L. Sombrio, D.L. Baptista, S.R. Teixeira, S.A.C. Carabineiro, C.G. Silva, J.L. Faria, Appl. Catal. A General 518 (2016) 198—205.
[9] Y.C. Chang, J.Y. Guo, Mater. Chem. Phys. 180 (2016) 9—13.
[10] A. Samad, M. Furukawa, H. Katsumata, T. Suzuki, S. Kaneco, J. Photochem. Photobiol. A Chem. 325 (2016) 97—103.
[11] A. Shirzadi, A. Nezamzadeh-Ejhieh, J. Mol. Catal. A Chem. 411 (2016) 222—229.
[12] E.D. Sherly, J.J. Vijaya, L.J. Kennedy, A. Meenakshisundaram, M. Lavanya, Korean J. Chem. Eng. 33 (4) (2016) 1431—1440.
[13] R. Cui, K. Shen, M. Xu, D. Xiang, Q. Xu, Mater. Sci. Semicond. Process. 43 (2016) 155—162.
[14] M. Lee, K. Yong, Nanotechnology 23 (19) (2012) 194014.
[15] Y. Cui, C. Wang, G. Liu, H. Yang, S. Wu, T. Wang, Mater. Lett. 65 (2011) 2284—2286.
[16] G.G. Untila, T.N. Kost, A.B. Chebotareva, Sol. Energy 127 (2016) 184—197.
[17] R. Pietruszka, R. Schifano, T.A. Krajewski, B.S. Witkowski, K. Kopalko, L. Wachnicki, E. Zielony, K. Gwozdz, P. Bieganski, E. Placzek-Popko, M. Godlewski, Sol. Energy Mater. Sol. Cells 147 (2016) 164—170.
[18] L. Chabane, N. Zebbar, M. Kechouane, M.S. Aida, M. Trari, Thin Solid Films 605 (2016) 57—63.
[19] B. He, J. Xu, H. Ning, H. Xiong, H. Xing, Y. Qin, Int. J. Nanosci. 15 (1) (2016) 1650014.
[20] T.J. Kuo, C.N. Lin, C.L. Kuo, M.H. Huang, Chem. Mat. 19 (2007) 5143—5147.
[21] M. Wang, K.E. Lee, S.H. Hahn, E.J. Kim, S. Kim, J.S. Chung, E.W. Shin, C. Park, Mater. Lett. 61 (2007) 1118—1121.
[22] X. Zhou, Q. Xue, H. Chen, C. Liu, Phys. E 42 (2010) 2021—2025.
[23] R. Pietruszka, G. Luka, K. Kopalko, E. Zielony, P. Bieganski, E. Placzek-Popko, M. Godlewski, Mater. Sci. Semicond. Process. 25 (2014) 190—196.